

# Modeling apparent Pb loss in zircon U-Pb geochronology

Glenn R. Sharman<sup>1</sup>, Matthew A. Malkowski<sup>2</sup>

<sup>1</sup>Department of Geosciences, University of Arkansas, Fayetteville, AR 72701, USA

<sup>2</sup>Department of Geological Sciences, Jackson School of Geosciences, University of Texas at Austin, Austin, TX 78712, USA

Correspondence to: Glenn R. Sharman (gsharman@uark.edu)

**Abstract.** Because the loss of radiogenic Pb from zircon is known to be a major factor that can cause inaccuracy in the U-Pb geochronological system, there is a need to better characterize the distribution of Pb loss in natural samples. Treatment of zircon by chemical abrasion (CA) has become standard practice in isotope dilution-thermal ionization mass spectrometry (ID-TIMS), but CA is much less commonly employed prior to *in-situ* analysis via laser ablation-inductively coupled plasma-mass spectrometry (LA-ICP-MS) or secondary ionization mass spectrometry (SIMS). Differentiating the effects of low levels of Pb loss in Phanerozoic zircon with relatively low precision *in-situ* U-Pb dates, where the degree of Pb loss is insufficient to cause discernible discordance, is challenging. We show that U-Pb isotopic ratios that have been perturbed by Pb loss may be modeled by convolving a Gaussian distribution that represents random variations from the true isotopic value stemming from analytical uncertainty with a distribution that characterizes Pb loss. We apply this mathematical framework to model the distribution of apparent Pb loss in 10 igneous samples that have both non-CA LA-ICP-MS or SIMS U-Pb dates and an estimate of the crystallization age, either through CA U-Pb or <sup>40</sup>Ar/<sup>39</sup>Ar geochronology. All but one sample showed negative age offsets that were unlikely to have been drawn from an unperturbed U-Pb date distribution. Modeling apparent Pb loss using the logit-normal distribution produced good fits with all 10 samples and showed two contrasting patterns in apparent Pb loss: samples where most zircon U-Pb dates undergo a bulk shift and samples where most zircon U-Pb dates exhibited low age offset but fewer dates had more significant offset. Our modeling framework allows comparison of relative degrees of apparent Pb loss between samples of different age, with the first and second Wasserstein distances providing useful estimates of the total magnitude of apparent Pb loss. Given that the large majority of *in-situ* U-Pb dates are acquired without the CA treatment, this study highlights a pressing need for improved characterization of apparent Pb loss distributions in natural samples to aid in interpreting non-CA *in-situ* U-Pb data and to guide future data collection strategies.

## 1 Introduction

Zircon U-Pb geochronology is arguably one of the most important radiometric dating approaches used by geoscientists, with widespread application to constraining the age of Pleistocene and older geologic materials (Davis et al., 2003; Schoene, 2013; Gehrels, 2014). We rely on zircon U-Pb dates for calibrating the geological time scale (e.g., Compston, 2000a; 2000b; Bowring and Schmitz, 2003; Gradstein et al., 2004; Kaufmann, 2006), constraining the timing of important Earth history events (Froude

30 et al., 1983; Schoene et al., 2010; Burgess et al., 2014), and determining the rates of Earth processes (Rioux et al., 2012;  
 31 Schoene et al., 2012; Johnstone et al., 2019). The zircon U-Pb geochronometer is particularly powerful due to the ability to  
 32 assess agreement between the  $^{238}\text{U} \rightarrow ^{206}\text{Pb}$  and  $^{235}\text{U} \rightarrow ^{207}\text{Pb}$  decay chains, with  $^{206}\text{Pb}^*/^{238}\text{U}$  and  $^{207}\text{Pb}^*/^{235}\text{U}$  dates in agreement  
 33 plotting on the Concordia line, where \* indicates radiogenic Pb (Wetherill, 1956).

34

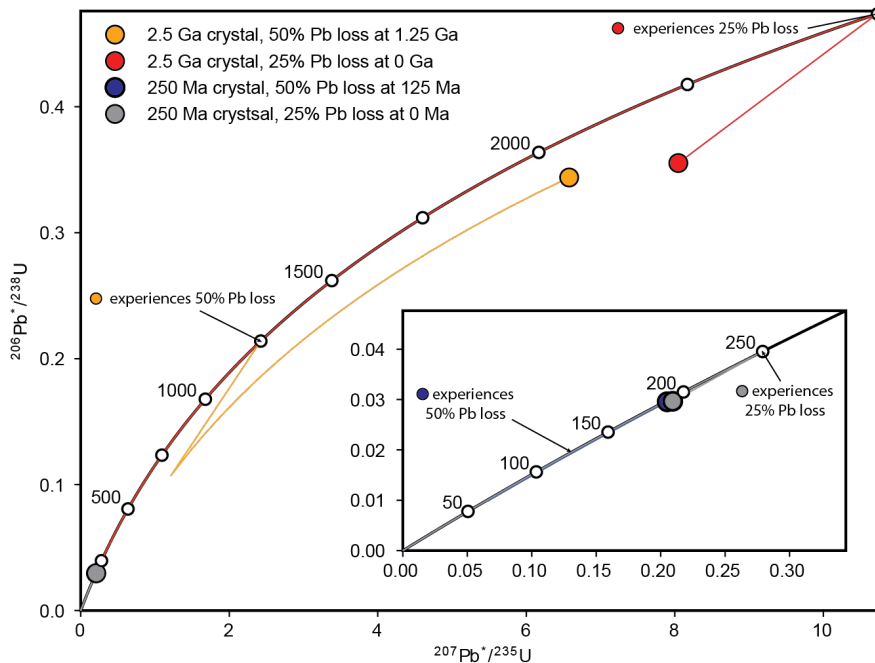


**Figure 1. Illustration of the influence of Pb loss on 250 Ma and 2.5 Ga zircon. Two Pb loss scenarios are shown: 25% loss at half the age of the zircon and 50% loss at present-day (0 Ma). The approximately linear nature of the  $^{206}\text{Pb}^*/^{238}\text{U}$  vs  $^{207}\text{Pb}^*/^{235}\text{U}$  Concordia line near the origin results in Pb loss producing limited discordance if the Pb loss occurs within several 100s of Myr of crystallization. Note that a greater amount of ancient Pb loss is required to produce the same shift in  $^{206}\text{Pb}^*/^{238}\text{U}$  relative to recent Pb loss. Thin, colored lines represent the path of each zircon.**

35

36

37 The causes and complications of open system behavior (e.g., radiogenic Pb loss) in zircon have long been a topic of study  
 38 (Tilton et al., 1955; Pidgeon et al., 1966). Although Pb loss events may be discerned on U-Pb Concordia diagrams in some  
 39 circumstances and can provide useful geologic information about the thermal and/or fluid flow history of a region (Silver and  
 40 Deutsch, 1963; Blackburn et al., 2011; Morris et al., 2015; Kirkland et al., 2017), recognizing Pb loss remains a challenge  
 41 when it occurs within several 100's Myr of crystallization (Fig. 1; Anderson et al., 2019). For example, due to the shape of the  
 42  $^{206}\text{Pb}^*/^{238}\text{U}$  versus  $^{207}\text{Pb}^*/^{235}\text{U}$  Concordia line, Pb loss in Phanerozoic zircon results in a 'sliding along concordia' effect that  
 43 can make Pb loss difficult to discern, particularly in relatively low-precision *in-situ* (i.e., LA-ICP-MS or SIMS) datasets when

44 the Pb loss produces concordant or only modestly discordant analyses (e.g., <10%; Ashwal et al., 1999; Bowring and Schmitz,  
45 2003; Ireland and Williams, 2003; Reimink et al., 2016; Spencer et al., 2016; Watts et al., 2016; Anderson et al., 2019). Such  
46 low levels of Pb loss have been termed ‘cryptic’ and may be associated with spatial heterogeneities including radiation-  
47 damaged U-rich zones and microstructures (Nasdala et al., 2005; Kryza et al., 2012; Watts et al., 2016). Most Pb loss in zircon  
48 is likely a consequence of recrystallization or Pb transport in crystals with severe radiation damage and exposure to  
49 hydrothermal alteration (Silver and Deutsch, 1963; Pidgeon et al., 1966; Mezger and Krogstad, 1997; Cherniak and Watson,  
50 2001; Marsellos and Garver, 2010). Mechanisms for Pb loss may include metamorphism (Kröner et al., 1994; Orejana et al.,  
51 2015; Zeh et al., 2016), hydrothermal alteration (Geisler et al., 2002, 2003); diagenetic fluids or fluid flow (Willner et al.,  
52 2003; Morris et al., 2015; Kirkland et al., 2020), and chemical weathering (Stern et al., 1966; Black, 1987; Balan et al., 2001;  
53 Pidgeon et al., 2017; Andersen and Elburg, 2022). Pb loss is thought to primarily occur at temperatures <250°C in which  
54 radiation damage in zircon is unable to be annealed over geologic timescales (Schoene, 2013).

55

56 Zircon domains that have lost Pb may be preferentially removed by first thermally annealing the zircon at high temperature  
57 (e.g., 800-1100°C) and then partially dissolving the zircon in a heated HF solution in a technique called chemical abrasion  
58 (CA) (Mattinson, 2005). The CA treatment is now routinely applied in ID-TIMS analysis and has contributed to both improved  
59 precision and accuracy of CA-ID-TIMS U-Pb data (Schoene, 2013). Although some *in-situ* U-Pb laboratories practice thermal  
60 annealing routinely (e.g., Allen and Campbell, 2012; Solari et al., 2015), CA has been applied much less frequently (Crowley  
61 et al., 2014; von Quadt et al., 2014; Watts et al., 2016; Ver Hoeve et al., 2018; Ruiz et al., 2022). Several studies that have  
62 conducted paired analysis of non-CA and CA of the same samples via *in-situ* U-Pb geochronology have found the non-CA U-  
63 Pb dates to skew younger than the CA U-Pb dates (Crowley et al., 2014; von Quadt et al., 2014; Watts et al., 2016). A growing  
64 number of maximum depositional age studies with tandem non-CA LA-ICP-MS and CA-ID-TIMS dating have shown the  
65 youngest non-CA U-Pb dates tend to be younger than expected relative to CA U-Pb dates or other geologic constraints, even  
66 when considering measurement uncertainty (e.g., Herriott et al., 2019; Schwartz et al., 2022; Howard et al., 2022; Sharman et  
67 al., 2023). However, there is a lack of quantitative constraints on the relative importance of Pb loss in influencing non-CA U-  
68 Pb date distributions acquired via *in-situ* mass spectrometry, particularly as related to influencing depositional age constraints  
69 (Copeland, 2020).

70

71 This study builds upon past research on open system behavior in zircon by presenting a mathematical framework for  
72 characterizing the distribution of apparent Pb loss on untreated (i.e., non-CA) U-Pb date distributions. We first suggest that U-  
73 Pb isotopic ratios that have been perturbed by Pb loss may be viewed as the convolution of two signals: a Gaussian distribution  
74 that reflects measurement uncertainty about the true isotopic ratio and the distribution that characterizes Pb loss. We then apply  
75 this mathematical framework to model the distribution of apparent Pb loss that has affected 10 igneous samples of Miocene to  
76 Carboniferous age. Our results highlight the importance of quantifying distributions of apparent Pb loss magnitude to better  
77 understand the potential influence on non-CA zircon U-Pb date distributions.

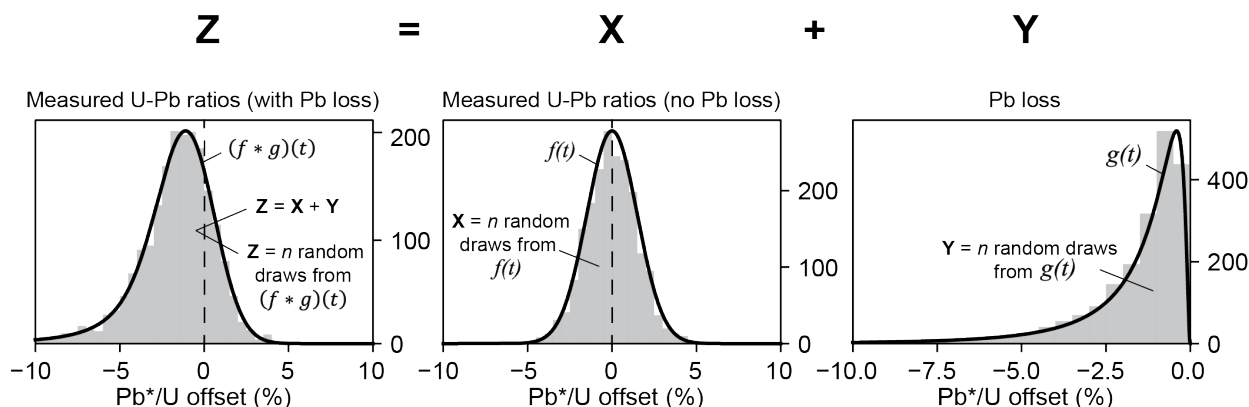


Figure 2. Illustration of how Pb\*/U isotopic ratios from  $n$  zircon analyses that have been perturbed by Pb loss ( $Z$ ) may be modeled as the summation of  $n$  non-perturbed Pb\*/U ratios ( $X$ ) and the amount of Pb loss encountered by each ( $Y$ ).  $X$  is drawn from  $f(t)$  that reflects the Gaussian distribution of Pb\*/U ratios that are unperturbed by Pb loss and  $Y$  is drawn from  $g(t)$  that represents the distribution of Pb loss in the sample. The distribution that characterizes  $Z$  may be found by convolving  $f(t)$  and  $g(t)$ . Although we assume that  $f(t)$  is a Gaussian distribution, the distribution type of Pb loss,  $g(t)$ , shown in this example as a logit-normal distribution ( $\mu=-4.5$ ,  $\sigma=1.0$ ) could take a number of discrete or continuous forms (Fig. 3). Note that in our modeling framework, values of  $X$ ,  $Y$ , and  $Z$  are normalized as percentage deviation from the true isotopic ratio (i.e., the mean of  $f(t)$ ), where negative values indicate that measured Pb\*/U is lower than the true ratio. See Supplemental Video 1 for an animation that illustrates the process of convolution and Supplemental Video 2 for an exploration of the logit-normal distribution in  $\mu$  and  $\sigma$  parameter space.

## 79 2 Mathematical framework

80 A series of  $n$  Pb\*/U measurements that have undergone Pb loss,  $Z$ , may be modeled as the sum of the corresponding  
81 unperturbed Pb\*/U values,  $X$ , and the amount that Pb\*/U changed due to Pb loss for each date,  $Y$ ,

$$82 \quad Z = X + Y \quad \text{(Equation 1)}$$

83 where  $Z$ ,  $X$ , and  $Y$  are all 1-D matrices with  $n$  values and units of percentage offset from the true isotopic value (Fig. 2).  
84 Because Pb loss produces a lower Pb\*/U ratio, the values of  $Y$  must be negative in our formulation of Equation 1. If  $X$  is drawn  
85 from a Gaussian distribution  $f(t)$  whose mean ( $\mu$ ) approximates the true isotopic value and whose standard deviation ( $\sigma$ ) reflects  
86 dispersion from the true value related to measurement uncertainty (e.g., Schoene et al., 2013) and if  $Y$  is drawn from a  
87 distribution that reflects Pb loss,  $g(t)$ , then  $Z$  may be viewed as being drawn from the convolution of  $f(t)$  and  $g(t)$

$$88 \quad (f * g)(t) = \int_{-\infty}^{\infty} f(\tau)g(t - \tau)d\tau \quad \text{(Equation 2)}$$

89 provided that  $X$  and  $Y$  are independent (Fig. 2; Supplemental Video 1). Convolution simply represents the summation of two  
90 random variables, in this case one related to analytical precision (i.e., random variation around the true isotopic value stemming  
91 from the measurement process) and the other related to the geologic process of Pb loss. We model Pb loss as percentage offset  
92 from the true Pb\*/U value rather than deviation in absolute time (i.e., Myr) to promote comparison of samples of different age  
93 (Fig. 2).

94  
95  
96  
97  
98  
99

Equation 2 may be solved analytically for some forms of  $f(t)$  and  $g(t)$ . For example, the convolution of Gaussian and exponential distributions is known as the exponentially modified Gaussian distribution (Grushka, 1972). However,  $(f * g)(t)$  may also be solved numerically, which has the advantage of allowing both  $f(t)$  and  $g(t)$  to take any form.

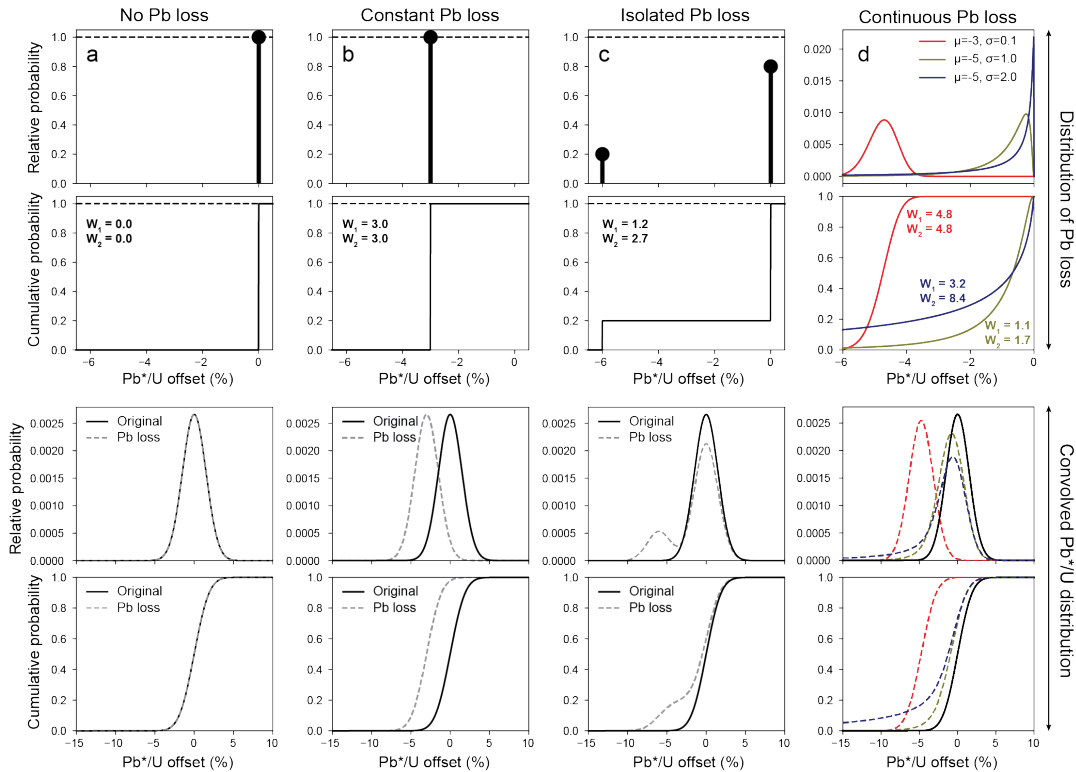


**Figure 3.** Illustration of how normally distributed zircon Pb\*/U values may be perturbed by discrete (a-c) or continuous (d) distributions of Pb loss. The top row represents the distribution of Pb loss in the sample expressed as a percentage of the true isotopic ratio (e.g.,  $^{206}\text{Pb}^*/^{238}\text{U}$  or  $^{207}\text{Pb}^*/^{235}\text{U}$ ) at the time of Pb loss, where the height of the black bar and ball indicates the relative probability of the specified Pb\*/U offset. Three discrete scenarios are shown: a) no Pb loss, b) constant Pb loss, and c) isolated Pb loss. A logit-normal distribution is shown as an example of continuous Pb loss in d). Additional examples of continuous Pb loss distributions are shown in Figure A1. The bottom row shows both the relative (above) and cumulative (below) probabilities of the unperturbed (solid black line) and Pb loss-perturbed (dashed line) Pb\*/U distributions.

00

## 01 **3 Methods**

### 02 **3.1 Modeling approach**

03 We use the mathematical framework described above to model both the distribution of apparent Pb loss,  $g(t)$ , experienced by  
04 a group of cogenetic crystals and their unperturbed U-Pb date distribution,  $f(t)$ . Because Pb loss is isotopically indiscriminate,  
05 Equation 2 may be equally applied to  $^{206}\text{Pb}^*/^{238}\text{U}$  and  $^{207}\text{Pb}^*/^{235}\text{U}$ . However, we model  $^{206}\text{Pb}^*/^{238}\text{U}$  ratios as these have much  
06 lower analytical uncertainty for the Carboniferous and younger samples analyzed in this study.

07  
08 To model  $g(t)$ , we allow the  $\mu$  of  $f(t)$  to vary within the 95% confidence interval associated with an independent estimate of  
09 the crystallization age. We then estimate both  $g(t)$  and  $\sigma$  of  $f(t)$  by iteratively solving for the combination of parameters that  
10 minimize the misfit between the measured  $\text{Pb}^*/\text{U}$  values and the modeled distribution  $(f * g)(t)$  using the Python  
11 `scipy.optimize.minimize()` function. We define misfit as the sum of squared residuals between the empirical cumulative  
12 distribution function (ECDF) of the measured  $\text{Pb}^*/\text{U}$  values and the cumulative density function (CDF) of the modeled  $\text{Pb}^*/\text{U}$   
13 distribution.

14  
15 If both non-CA and CA analyses are available from the same sample, then the distribution of CA U-Pb dates may be used to  
16 constrain the parameters of  $f(t)$ . For such samples, we modify the approach described above by first finding the Gaussian  
17 distribution  $f(t)$  that most closely approximates the treated  $\text{Pb}^*/\text{U}$  distribution. We then use this best-fitting  $f(t)$  in estimating  
18  $g(t)$  using the minimization-of-misfit technique described above. Such datasets have the advantage of providing constraints on  
19  $\sigma$  of  $f(t)$ , which is otherwise treated as an unknown parameter during modeling if only non-CA U-Pb dates are available.

20  
21 In order to estimate  $g(t)$  as described above, we must choose one or more reasonable parametric models that are appropriate  
22 for describing distributions of Pb loss. One possibility is that all zircon crystals in the sample experienced the same amount of  
23 Pb loss, which could shift  $\text{Pb}^*/\text{U}$  from 0% to -100% of its value. Such a scenario of constant Pb loss may be modeled by a  
24 discrete form of  $g(t)$  where a single parameter specifies the percentage of Pb lost. Convolution of such a discrete form of  $g(t)$   
25 simply produces a negative shift in the  $\text{Pb}^*/\text{U}$  values (i.e., Fig. 3b).

26  
27 Another possibility is that Pb loss was experienced by only a subset of crystals (i.e., isolated Pb loss). This scenario may also  
28 be modeled by assigning  $g(t)$  to a discrete distribution with two parameters: one that indicates the fraction of Pb lost and one  
29 that specifies the proportion of crystals that underwent Pb loss (Fig. 3c). This parameterization of  $g(t)$  will produce a bimodal  
30 pattern in U-Pb values, particularly if the degree of Pb loss is significant relative to measurement uncertainty (Fig. 3c).

31  
32 Instead of modeling  $g(t)$  as a discrete distribution where Pb loss is restricted to certain values, we may also consider a  
33 continuous probability distribution where values of Pb loss can take on any value between 0% and 100% (Fig. 3d). Rather than

34 assume *a priori* the form(s) that  $g(t)$  might take, we considered a wide range of 1- or 2-parameter distributions for the purposes  
 35 of exploratory modeling (Appendix A). Of the distribution types considered, we identified the logit-normal distribution, also  
 36 known as the logistic normal distribution, as perhaps the most reasonable for modeling Pb loss. The logit-normal distribution  
 37 has the property of having a logit (i.e., the quantile function of the logistic distribution) that is normally distributed with a  
 38 geometric mean of  $\mu$  and standard deviation of  $\sigma$  (Aitchison and Shen, 1980; Mead, 1965)

$$39 \quad f(x, \mu, \sigma) = \frac{1}{\sigma\sqrt{2\pi}} \frac{1}{x(1-x)} e^{-\frac{(\text{logit}(x)-\mu)^2}{2\sigma^2}} \quad (\text{Equation 3})$$

40 for  $0 < x < 1$ . The logit-normal distribution is well-suited for modeling constrained data types (e.g., compositional data; Aitchison  
 41 and Bacon-Shone, 1999; Vermeesch, 2018b) in part due to it being defined  
 42 over  $0 < x < 1$ . We invert and scale the distribution to extend from -  
 43  $100\% < x < 0\%$  to match the sign and units of Pb\*/U offset due to Pb loss  
 44 when expressed as a percentage (Fig. 3d).

45  
 46 Figure 4 explores the relationship of the logit-normal distribution to its  
 47 two parameters ( $\mu$  and  $\sigma$ ) (see also Supplemental Video 2). The  
 48 distribution has a ‘spikey’ character when  $\sigma$  is a very small number (e.g.,  
 49 0.001; Fig. 4a), which would be a reasonable approximation for samples  
 50 that underwent an approximately constant amount of Pb loss (e.g., Figs.  
 51 3a and 3b). Although the logit-normal distribution cannot model 0% or  
 52 100% Pb loss, these values may be approximated by making  $\mu$  a large  
 53 negative or positive number, respectively. A sample where most zircon  
 54 exhibit very little Pb loss but with fewer zircon experiencing significant  
 55 Pb loss could be produced by  $\mu = -4$  and  $\sigma = 1.0$  (Fig. 4c). Alternatively,  
 56 a sample with a peak probability of Pb\*/U offset  $< 0\%$  may be modeled  
 57 using moderate values of  $\sigma$  (e.g., 0.25-1; Figs. 4b and 4c). The logit-  
 58 normal distribution produces bimodal distributions where most probability  
 59 is close to 0% and -100% when  $\sigma$  values are high (e.g.,  $\gg 1$ ; Fig. 4d).

### 60 3.2 Samples

61 We apply the mathematical and modeling framework presented above to estimate the distribution of apparent Pb loss in 10  
 62 igneous samples that range in age from Carboniferous to Miocene, nine of which have been published previously (Table 1).  
 63 Samples CTU, RCP, and SRF are all from upper Eocene rhyolites of the Caetano caldera system of the western United States  
 64 (Watts et al., 2016). These samples were split into non-CA and CA aliquots prior to analysis via SIMS (Watts et al., 2016).  
 65 We used the error-weighted mean age of the CA U-Pb dates as an estimate of the true crystallization age for each sample, with

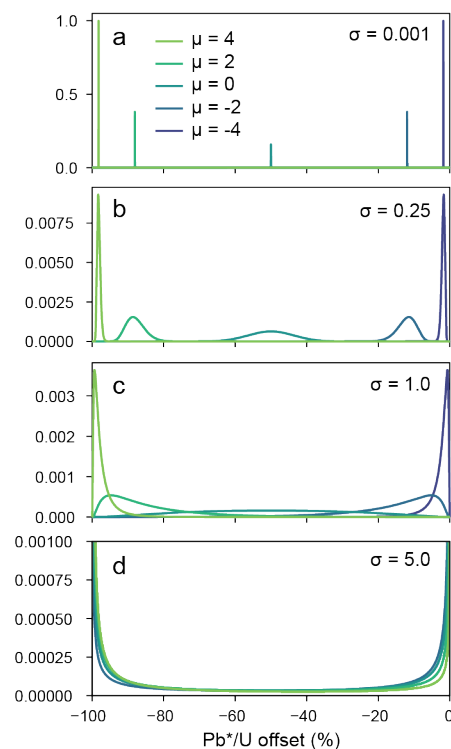


**Figure 4. Exploration of the logit-normal distribution's parameter space. Note that we have rescaled the x-axis of the logit-normal distribution such that  $-100 < x < 0$ .**

66 weighted means approximately 0.4-0.6 Myr older than the corresponding  $^{40}\text{Ar}/^{39}\text{Ar}$  sanidine ages (Watts et al., 2016). The  
67 number of analyses per aliquot (non-CA or CA) ranges from 17-34 for these three samples (Table 1).  
68

**Table 1. Sample Summary**

Sample	Age (Ma)	Reference	N (non- CA)	N (CA)	Model results (best fit logit-normal distribution)					
					$f(t)$ (Ma)	$g(t)$ sum of squared residuals	$g(t)$ parameters	$g(t)$ P2.5-P50- P97.5 (%)	$W_1$	$W_2$
ELM18 DVTC- 10	15.7 $\pm 0.2$ ( $2\sigma$ ) <sup>1</sup>	Miller et al. (2022)	144	n.a.	15.90 $\pm$ 0.55 ( $1\sigma$ )	1.0	$\mu = -3.24$ $\sigma = 1.28$	-32.49 -3.77 -0.32	6.9	11.1
248-2	24.422 $\pm 0.25$ ( $2\sigma$ ) <sup>3</sup>	von Quadt et al. (2014)	30	55	24.42 $\pm$ 0.64 ( $1\sigma$ )	2.7	$\mu = -4.48$ $\sigma = 1.06$	-8.3 -1.12 -0.14	1.9	3.0
029-5 <sup>5</sup>	24.480 $\pm 0.084$ ( $2\sigma$ ) <sup>3</sup>	von Quadt et al. (2014)	42	48	24.47 $\pm$ 0.79 ( $1\sigma$ )	3.3	$\mu = -3.10$ $\sigma = 0.47$	-10.17 -4.31 -1.76	4.7	5.2
059-1 <sup>5</sup>	24.57 $\pm 0.28$ ( $2\sigma$ ) <sup>2</sup>	von Quadt et al. (2014)	41	36	24.50 $\pm$ 0.95 ( $1\sigma$ )	1.1	$\mu = -3.48$ $\sigma = 0.52$	-7.87 -2.99 -1.1	3.4	3.8
CTU	34.41 $\pm 0.26$ ( $2\sigma$ ) <sup>2</sup>	Watts et al. (2016)	24	18	34.47 $\pm$ 0.83 ( $1\sigma$ )	2.1	$\mu = -3.21$ $\sigma = 0.29$	-6.65 -3.88 -2.23	4.0	4.2
RCP	34.38 $\pm 0.32$ ( $2\sigma$ ) <sup>2</sup>	Watts et al. (2016)	34	18	34.19 $\pm$ 0.75 ( $1\sigma$ )	3.1	$\mu = -3.96$ $\sigma = 0.80$	-8.38 -1.87 -0.40	2.5	3.3
SRF	34.62 $\pm 0.37$ ( $2\sigma$ ) <sup>2</sup>	Watts et al. (2016)	17	17	34.25 $\pm$ 0.75 ( $1\sigma$ )	5.1	$\mu = -4.57$ $\sigma = 1.08$	-7.92 -1.03 -0.12	1.8	2.9
DG 026	76.41 $\pm 0.45$ ( $2\sigma$ ) <sup>3</sup>	von Quadt et al. (2014)	31	34	76.16 $\pm$ 1.42 ( $1\sigma$ )	3.0	$\mu = -3.74$ $\sigma = 0.56$	-6.65 -2.32 -0.79	2.7	3.1
MM20- EC- 109 <sup>6</sup>	144.50 $\pm 0.07$ ( $2\sigma$ ) <sup>4</sup>	This study	68	n.a.	144.43 $\pm$ 3.12 ( $1\sigma$ )	1.6	$\mu = -4.73$ $\sigma = 1.91$	-27.16 -0.87 -0.02	3.6	8.8
AvQ 244 <sup>7</sup>	333.60 $\pm 0.66$ ( $2\sigma$ ) <sup>3</sup>	von Quadt et al. (2014)	17	19	333.64 $\pm$ 10.86 ( $1\sigma$ )	12.3	$\mu = -2.69$ $\sigma = 0.82$	-25.30 -6.36 -1.34	8.1	10.3

69  
70 <sup>1</sup>Sanidine  $^{39}\text{Ar}/^{40}\text{Ar}$  age (Snow and Lux, 1999)  
71 <sup>2</sup>Error-weighted mean of chemically abraded U-Pb dates  
72 <sup>3</sup>Concordia age (CA-ID-TIMS)  
73 <sup>4</sup>Error-weighted mean 5 of 5 zircon crystals analyzed via CA-ID-TIMS  
74 <sup>5</sup>U-Pb dates older than 28 Ma excluded from analysis  
75 <sup>6</sup>U-Pb dates older than 158 Ma excluded from analysis  
76 <sup>7</sup>U-Pb dates older than 360 Ma excluded from analysis  
77 N = Number of analyses  
78 n.a. = Not available  
79  $W_1$  = first Wasserstein distance  
80  $W_2$  = second Wasserstein distance  
81



82 We present analysis of five samples reported in von Quadt et al. (2014), including upper Oligocene andesite/trachy-andesite  
83 from Macedonia (248-2, 029-5, and 059-1), upper Cretaceous dolerite from Romania (DG 026), and middle Carboniferous  
84 granite from West-Bulgaria (AvQ 244). These samples were also split into non-CA and CA aliquots prior to analysis via LA-  
85 ICP-MS. For samples other than 059-1 we use concordia ages from CA-ID-TIMS analyses of between three and six crystals  
86 for the crystallization age of each sample (von Quadt et al., 2014; Table 1). For sample 059-1 we used the weighted mean of  
87 the CA U-Pb dates. The number of analyses per sample (non-CA or CA) ranged from 17-55 for this dataset (Table 1).

88

89 Sample ELM18DVTC-10 is from a Miocene ash-flow tuff from the Pangua Formation in the western United States that has  
90 144 U-Pb dates acquired via LA-ICP-MS (Miller et al., 2022). We use a  $^{40}\text{Ar}/^{39}\text{Ar}$  weighted mean age of  $15.7 \pm 0.2$  Ma ( $2\sigma$ )  
91 from the same unit as an estimate of the crystallization age of this sample (sample 592-GV1 of Snow and Lux, 1999). Sample  
92 ELM18DVTC-10 was highlighted by Schwartz et al. (2022) who noted the youngest zircon U-Pb dates to be much younger  
93 than the accepted  $^{40}\text{Ar}/^{39}\text{Ar}$  age of this unit. Miller et al. (2022) also noted the presence of these young zircon and suggested  
94 that they may be a consequence of surface contamination from units higher in the section.

95

96 Sample MM20-EC-109 is a Lower Cretaceous intermediate ash interbedded within marine carbonaceous mudstone from the  
97 Rio Mayer Formation of Argentina with 68 zircon U-Pb dates acquired via LA-ICP-MS (Table A3). Laser ablation spot  
98 locations were selected on the rim and/or core of the zircon guided by CL images (Figure A3), with 59 zircon crystals analyzed  
99 in total. We use a crystallization age of  $144.43 \pm 0.07$  Ma ( $2\sigma$ ) derived from a weighted mean of five zircon crystals analyzed  
00 via CA-ID-TIMS at the Boise State University Isotope Geology Laboratory (Table A4). This sample exhibits a large offset  
01 between the youngest U-Pb dates acquired via LA-ICP-MS, up to ~60% younger than the CA-ID-TIMS weighted mean.

### 02 **3.3 Statistical analysis**

03 To evaluate the likelihood that the measured  $\text{Pb}^*/\text{U}$  distribution could have been drawn from the modeled  $(f * g)(t)$ , we apply  
04 the nonparametric, 1-sided Kolmogorov-Smirnov (K-S) and Kuiper statistical tests that compare the ECDF with the cumulative  
05 CDF of  $(f * g)(t)$  (Press, 2007). The Kuiper statistic is relatively more sensitive in differences in the tails of the distributions  
06 versus the K-S statistic (Vermeesch, 2018a). We reject the null hypothesis that the non-CA U-Pb dates were drawn from  $(f * g)(t)$   
07 if the K-S or Kuiper p-value is  $<0.05$  (i.e., 95% confidence level). We thus interpret p-values  $>0.05$  to indicate that the  
08 non-CA U-Pb dates could have been plausibly drawn from  $(f * g)(t)$  at a 95% confidence level (Press, 2007). However, it  
09 should be noted that Saylor and Sundell (2016) found that both K-S and Kuiper p-values more frequently reject the null  
10 hypothesis than expected. We thus use p-values as a general guideline to model goodness-of-fit.

11

12 The Wasserstein distance has been recently proposed as a metric for quantifying the dissimilarity between detrital zircon U-  
13 Pb age distributions (Lipp and Vermeesch, 2023). We consider the first and second Wasserstein distances,  $W_1$  and  $W_2$ , to be  
14 useful approximations for the total degree of negative  $\text{Pb}^*/\text{U}$  perturbation that a set of analyses has experienced,

15 
$$W_1 = \int_0^1 |M^{-1} - N^{-1}| dt \quad (\text{Equation 3})$$

16 
$$W_2 = \sqrt{\int_0^1 |M^{-1} - N^{-1}|^2 dt} \quad (\text{Equation 4})$$

17 where  $M^{-1}$  and  $N^{-1}$  are the inverses of the CDFs  $M$  and  $N$ . Because values of Pb loss are restricted to between 0% and 100%,  
18 both  $W_1$  and  $W_2$  yield maximum possible values of 100 (i.e., 100% of analyses have -100% Pb\*/U offset, or the U-Pb system  
19 is completely reset). The  $W_1$  simply equates to the area beneath the cumulative probability distribution of  $g(t)$  (e.g., Fig. 3).  
20 Because the  $W_2$  distance involves a squaring of the distance between the quantile functions, it imparts a higher cost penalty for  
21 the part of the distribution with strongly offset values. For example, the  $W_1$  and  $W_2$  distances are equal for a Pb loss function  
22 characterized by constant Pb loss (e.g., 3% Pb loss produces  $W_1$  and  $W_2$  values of 3, Fig. 3b). However, the  $W_2$  distance is  
23 often much larger than  $W_1$  for Pb loss distributions with a heavy tail (Fig. 3d). As such, the  $W_2/W_1$  ratio provides an  
24 approximation of Pb loss distribution asymmetry, with values of 1 indicating constant Pb loss and values  $\gg 1$  indicating highly  
25 asymmetric Pb loss.

#### 26 **4 Results**

27 Of the four primary types of Pb loss distributions considered (Fig. 3), the logit-normal distribution yielded the lowest average  
28 misfit with a value of 3.5, followed by the isolated Pb loss scenario (average of 4.5) and the constant Pb loss scenario (average  
29 of 10.5) (Table A2). The scenario of no Pb loss performed the worst of any scenario that we considered, with an average misfit  
30 of 101.3 (Table A2). Correspondingly, both K-S and Kuiper p-values for the no Pb loss  
31

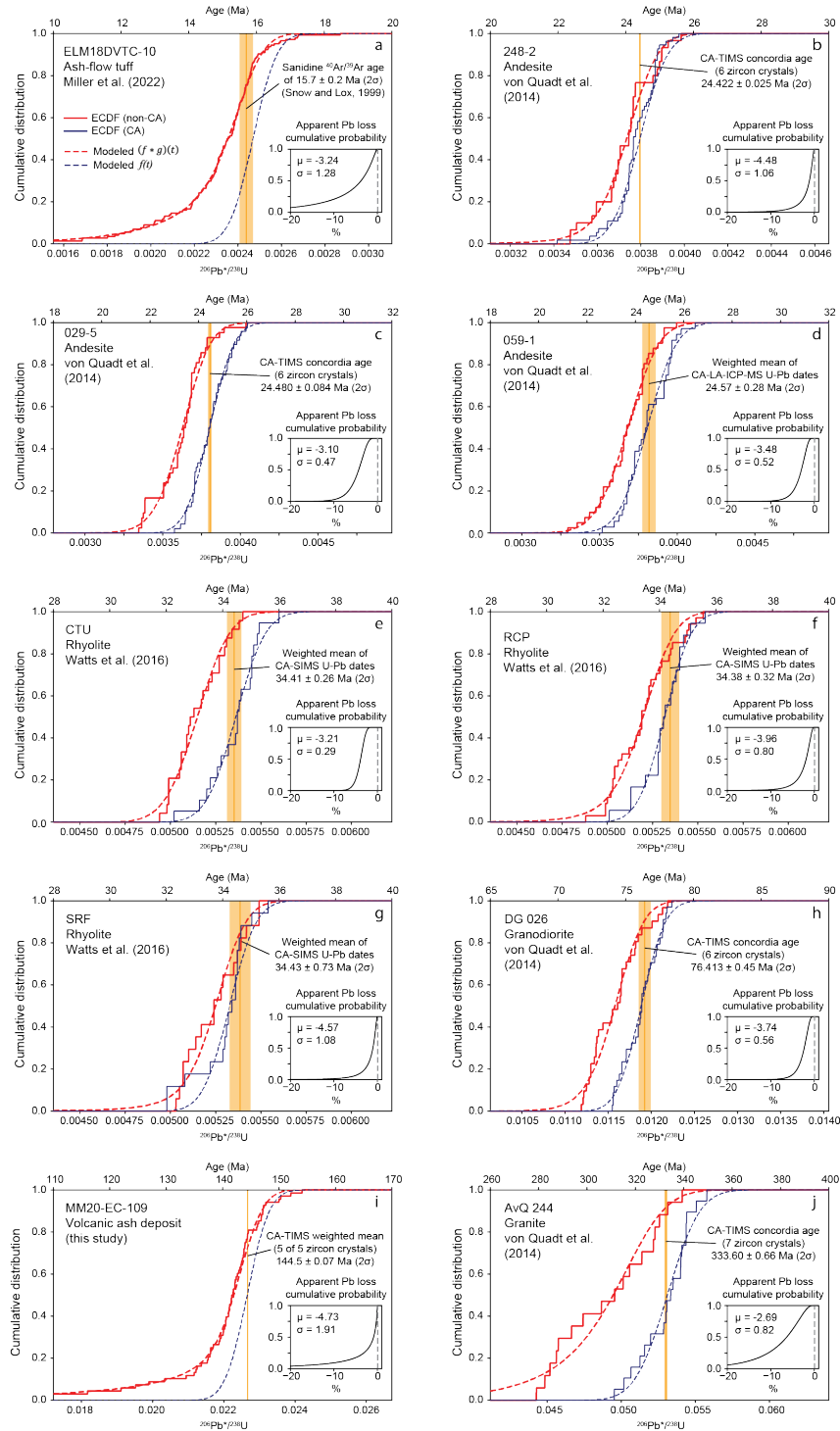


**Figure 5. Modeling of apparent Pb loss in zircon U-Pb dates acquired via LA-ICP-MS or SIMS. The best-fitting logit-normal distribution of apparent Pb loss is shown (Table 1; see Figure A1 for plots of all samples and apparent Pb loss distribution types modeled). Empirical cumulative distribution functions (ECDFs) are shown as solid lines while model results are shown as dashed lines. See text for further discussion of model results.**

32

33 scenario are  $\ll 0.05$  for all samples except SRF, suggesting that the untreated LA-ICP-MS or SIMS U-Pb dates are unlikely  
34 to have been drawn from an unperturbed U-Pb date distribution.

35

36 Figure 5 presents a comparison of actual versus modeled U-Pb date distributions for each sample, with the best-fitting logit-  
37 normal distribution shown (Table 1; see Figure A1 for individual plots that show the fit for each sample and distribution type).

38 We chose to not consider discrete distributions of  $g(t)$  for the “best” fit because we consider it unlikely that Pb loss (or other  
39 processes that cause negative age offsets) would be limited to discrete values (e.g., Fig. 3). Values of  $\mu$  for  $g(t)$  ranged from -  
40 2.69 to -4.73 with corresponding values of  $\sigma$  spanning 0.29 to 1.91.  $W_1$  distances ranged between 1.8 (sample SRF) and 8.1  
41 (sample AvQ 244) and  $W_2$  distances between 2.9 and 11.1 (Table 1; Fig. 5).

42

43 A plot of the best-fitting logit-normal distributions displays two distinct behaviors of  $g(t)$  (Fig. 6). (1) Four samples with  $\mu <$   
44  $\sim -3$  and  $\sigma > 1$  and have a  $g(t)$  maximum relative probability close to 0% suggesting a strongly decaying rate of offset (i.e.,  
45 most zircon experienced very little Pb loss, while a few have more significant Pb\*/U offset). These samples also displayed  
46  $W_2/W_1 \geq 1.6$ . (2) The remaining six samples that yielded  $\sigma < 1$  and generally higher  $\mu$  values ( $> -4$ ) displayed a tendency for  
47 the mode of  $g(t)$  to be  $> 0\%$ , representing more of a bulk shift in age (e.g., most U-Pb dates have some offset, while relatively  
48 few have very little or very much age offset). These samples produced  $W_2/W_1 \leq 1.3$ .

## 49 5 Discussion

### 50 5.1 Assumptions and limitations

51 The mathematical and modeling framework that we present includes  
52 several underlying assumptions and limitations that should be  
53 considered.

54  
55 1. Because  $g(t)$  could represent any geological or analytical  
56 process that introduces negative age offsets, we use the phrase “apparent  
57 Pb loss” when describing our modeled estimates of  $g(t)$ . For instance,  
58 matrix-related systematic errors (Allen and Campbell, 2012), addition of  
59 U-Th during weathering (Pigeon et al., 2019), and even sample  
60 contamination from younger minerals could introduce negative age shifts  
61 exclusive of loss of radiogenic Pb. Common Pb corrections, particularly  
62 the  $^{207}\text{Pb}$ -correction, may also introduce a bias towards artificially low  
63  $\text{Pb}^*/\text{U}$  values (Anderson, 2002; Anderson et al., 2019). We recommend  
64 that these additional complexities in the U-Pb system be considered when  
65 interpreting modeled estimates of  $g(t)$  as representing distributions of Pb  
66 loss.

67  
68 2. Our approach of parameterizing  $g(t)$  for the purpose of  
69 exploratory modeling has the advantage of yielding results that are  
70 interpretable while also being suitable for the relatively low- $n$  datasets  
71 available. However, any parametric model is likely a simplification of the  
72 true  $g(t)$ , and thus we consider our modeled estimates of  $g(t)$  to be first-order approximations. Analyzing a greater range of  
73 samples with a greater number of  $\pm\text{CA}$  *in-situ* U-Pb analyses, with ideal datasets having 100s or even 1000s of analyses per  
74 sample (e.g., Pullen et al., 2014; Sundell et al., 2021), would likely improve our ability to constrain the form(s) of  $g(t)$  and  
75 evaluate whether the logit-normal distribution or other forms of  $g(t)$  are appropriate. Such datasets would also be more  
76 amenable to nonparametric solutions of estimating  $g(t)$ .

77  
78 3. For  $g(t)$  to represent the true distribution of Pb loss, the process of convolution must be applied to  $\text{Pb}^*/\text{U}$  ratios at the  
79 time of Pb loss. Because  $\text{Pb}^*$  is progressively added to the crystal over time, a greater amount of ancient Pb loss is required to  
80 achieve the same reduction in  $\text{Pb}^*/\text{U}$  relative to recent Pb loss. This point is illustrated in Figure 1 where a 50% reduction in  
81  $\text{Pb}^*$  at 125 Myr after crystallization produces a similar reduction in  $^{206}\text{Pb}^*/^{238}\text{U}$  when compared to zircon of the same age that

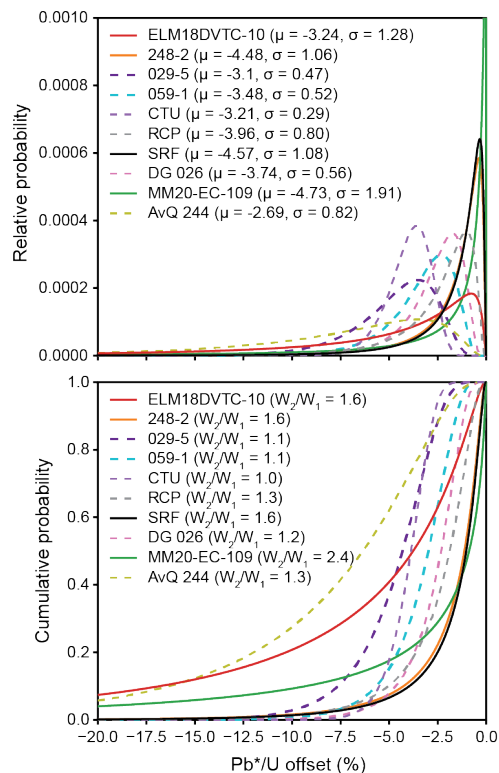


**Figure 6. Distributions of apparent Pb loss when modeled as a logit-normal distribution. Samples with  $\sigma < 1$  are shown as a dashed line.**

82 lost 25% of its Pb\* at 250 Myr (present day). For this reason,  $g(t)$  can be viewed as a minimum estimate in the case of ancient  
83 Pb loss. If the timing of Pb loss is known or can be estimated (e.g., Morris et al., 2015), the input Pb\*/U ratios can be adjusted  
84 prior to analysis such that  $g(t)$  more accurately reflects the true magnitude of Pb loss.

85

86 4. The modeling framework presented above is designed for a group of cogenetic crystals with a shared crystallization  
87 age (e.g., autocrystic zircon from the same magmatic episode; Miller et al., 2007). This requirement stems from our definition  
88 of apparent Pb loss as a relative shift, or percentage deviation from the true isotopic value (Fig. 2). The assumption that all  
89 zircon are coeval is a simplification, as even autocrystic zircon crystallize over a period of time, typically  $10^3$ - $10^4$  yr timescales  
90 (Miller et al., 2007; Rossignol et al., 2019). Multimodal detrital samples or igneous samples with xenocrystic or inherited  
91 zircon are not easily modeled because these samples would violate our assumption of a shared crystallization age. Failure to  
92 recognize the true heterogeneity in crystallization age in such a sample could cause an incorrect interpretation of the apparent  
93 Pb loss distribution.

94

95 5. For datasets with paired non-CA and CA measurements, our modeling approach assumes that the relative precision  
96 of the analyses is similar. This is because the Gaussian distribution that best approximates the CA U-Pb date distribution,  $f(t)$ ,  
97 is convolved with the apparent Pb loss distribution  $g(t)$  to fit the non-CA U-Pb date distribution. The Watts et al. (2016) SIMS  
98 dataset shows similar relative precision regardless of treatment approach (non-CA versus CA). Some samples from the von  
99 Quadt et al. (2014) LA-ICP-MS dataset exhibit slightly lower relative precisions for non-CA versus CA, with sample AvQ  
00 244 yielding the largest difference with an average relative precision of 1.1% ( $1\sigma$ ) for non-CA dates and 0.8% ( $1\sigma$ ) for CA  
01 dates. We suggest that for the purposes of modeling apparent Pb loss, paired non-CA and CA U-Pb datasets should be collected  
02 on the same instrument using similar acquisition parameters to avoid introducing large changes in measurement precision.  
03 Alternatively, the CA U-Pb dates may be used to only constrain the  $\mu$  of  $f(t)$  in the model, with  $\sigma$  treated as an unknown  
04 parameter (e.g., for paired non-CA LA-ICP-MS and CA-ID-TIMS datasets; Figs. 5a and 5i).

05

06 6. For datasets with paired non-CA and CA measurements, we do not consider any imperfections of the chemical  
07 abrasion process. For example, although the CA treatment aims to completely remove all radiation damaged zones of the  
08 crystal (Mattinson, 2005), it is possible to have remaining residual zones of Pb loss following treatment (e.g., Schoene et al.,  
09 2010). Any such remaining compromised domains of the crystal will yield at least some apparent Pb loss when analyzed. For  
10 instance, Watts et al. (2016) interpreted three zircon U-Pb analyses from SRF to have some residual Pb loss that was not fully  
11 accounted for by the CA process (Fig. 5g). Incorporation of Pb loss-perturbed U-Pb dates when modeling  $f(t)$  would likely  
12 produce an underestimate of the true magnitude of the apparent Pb loss.

13

14

15

## 16 5.2 Distributions of apparent Pb loss

17 What distribution type(s) characterize apparent Pb loss in natural samples? Our results strongly suggest that at least nine of the  
18 10 samples modeled have at least some systematic negative offset in  $^{206}\text{Pb}^*/^{238}\text{U}$  that cannot be explained by random  
19 measurement uncertainties alone. This is because the K-S and Kuiper statistical tests are unable to reject the null hypothesis  
20 for many of the apparent Pb loss distribution types considered (Table A1). For example, only the no Pb loss scenario produced  
21 a  $p$ -value  $< 0.05$  for sample MM20-EC-109, suggesting that any of the other modeled distributions of apparent Pb loss may be  
22 statistically plausible for this sample. These results suggest that we cannot confidently distinguish between discrete (constant  
23 or isolated) or continuous distributions of apparent Pb loss in the datasets modeled. Except for ELM18DVTC-10 which has  
24 144 non-CA LA-ICP-MS analyses, the samples we analyzed have relatively low numbers of analyses (between 17 and 68,  
25 average of 32) for a given sample and treatment category (non-CA or CA) (Table 1). We suspect that collection of larger- $n$   
26 datasets would allow better resolution of which parameterizations of  $g(t)$  might be most appropriate.

27

28 Even if the specific distribution type(s) that characterizes  $g(t)$  cannot be uniquely identified, our analysis suggests two  
29 contrasting behaviors in apparent Pb loss (Fig. 6). We speculate that U-Pb dates that undergo a bulk shift (i.e.,  $W_2/W_1 \cong 1$ )  
30 may reflect a population of zircon crystals with relatively homogenous characteristics (e.g., size, U content, etc.) that have all  
31 experienced a similar post-crystallization history. Correspondingly, the population of zircon that produces U-Pb dates with a  
32 highly asymmetric distribution of age offset (i.e.,  $W_2/W_1 > \sim 1.5$ ) may reflect heterogeneity between crystals, with variable  
33 characteristics. For example, Pb loss is thought to be promoted in small zircon crystals and in zircon with elevated U (Ashwal  
34 et al., 1999; Gehrels et al., 2020), and thus distributions of particle size and/or trace element geochemistry may influence  
35 asymmetric patterns in  $g(t)$ . Collection of size measurements and trace element concentrations from zircon in addition to  
36 measurement of the U-Pb date (e.g., Watts et al., 2016) would likely help evaluate hypotheses about the underlying factors  
37 that influence apparent Pb loss distributions. Furthermore, given the relatively small number of samples modeled in this study,  
38 we suggest that there is a need for more samples to undergo paired non-CA and CA characterization to improve understanding  
39 of the range of behaviors that may be typical. For example, it is presently unclear whether it is more common for samples to  
40 have their U-Pb dates bulk shifted (e.g., samples 029-5, 059-1, CTU, DG 026) versus having relatively few U-Pb dates highly  
41 offset (e.g., samples MM20-EC-109 and ELM18DVTC-10; Fig. 5).

42

43 Why do some samples experience more overall apparent Pb loss than others? Although we anticipated that apparent Pb loss  
44 would be greater for older samples, our analysis shows no clear trend by sample age (although we acknowledge that the  
45 relatively high degree of apparent Pb loss modeled in the youngest sample, ELM18DVTC-10, may be a consequence of  
46 contamination from overlying units, instead of true Pb loss; Miller et al., 2022). Even the three samples from the same Eocene  
47 caldera system (CTU, RCP, and SRF) showed contrasting amounts of apparent Pb loss ( $W_2$  ranges from 2.9 to 4.2; Table 1)

48 as noted by Watts et al. (2016). Characterizing the overall magnitude of apparent Pb loss in a wider range of samples would  
49 likely help elucidate predictive factors, if any.

50

### 51 **5.3 Importance of quantifying the distribution of apparent Pb loss in *in-situ* U-Pb geochronology**

52 The overwhelming majority of published *in-situ* U-Pb dates from zircon, minimally >600,000 and likely in the millions of  
53 analyses (Puetz et al., 2021), have not been treated using CA. In contrast, CA is now practiced routinely in the ID-TIMS  
54 community which has contributed to growing precision and accuracy over the past two decades (Schoene, 2013). However,  
55 the strategy of mitigating Pb loss through avoidance is perhaps less easily adopted to routine *in-situ* U-Pb geochronology. For  
56 instance, there may be practical limitations with chemically abrading large numbers of zircon crystals, including the potential  
57 loss of certain age modes that would be detrimental to provenance analysis. We thus suggest that there is a pressing need to  
58 improve quantitative characterization of apparent Pb loss distributions in non-CA *in-situ* U-Pb datasets to aid in interpreting  
59 these datasets and to guide strategies for future data collection.

60

61 It is somewhat concerning that nine of the 10 samples analyzed in this study exhibited statistically significant amounts of  
62 negative age offset from the estimated true crystallization age. Even a small age offset of a few percent, or cryptic Pb loss  
63 (Kryza et al., 2012; Watts et al., 2016), has potentially important repercussions for interpreting the age and rates of geologic  
64 events and processes. For example, there is a growing awareness in the detrital geochronological community that the youngest  
65 zircon U-Pb dates often skew unexpectedly young relative to the plausible crystallization age (e.g., Herriot et al., 2019; Gehrels  
66 et al., 2020; Schwartz et al., 2022). Presently, there is no consensus on the importance of post-depositional Pb loss on  
67 influencing depositional age interpretations (e.g., Herriott et al., 2019; Copeland, 2020; Schwartz et al., 2022). Sample MM20-  
68 EC-109 illustrates the risk well; we initially interpreted the young tail on the U-Pb date distribution to suggest a depositional  
69 age of ~125 Ma based on the youngest cluster of overlapping U-Pb dates. The youngest single analysis was a  $60.5 \pm 2.4$  Ma  
70 rim on a  $135.3 \pm 3.0$  Ma core, with the second youngest being a  $79 \pm 1.2$  Ma date measured from the core of a zircon crystal,  
71 with the corresponding rim yielding an older  $129.8 \pm 3.6$  Ma date (Table A2). Interpretation of the youngest single U-Pb date  
72 or dates as the depositional age of this sample would have produced a highly erroneous estimate, off by up to -58% of the true  
73 eruption age of  $144.50 \pm 0.07$  ( $2\sigma$ ) Ma as determined by CA-ID-TIMS. Because this ash is interbedded within a sequence of  
74 organic rich marine mudstone in the Austral Basin of Argentina, the misinterpretation in this case could have led to an  
75 erroneous depositional age model with implications for interpreting the paleoclimatic and geodynamic context of these  
76 sediments.

77

78 Although modeling detrital samples was outside of the scope of this study, we believe that our results bear upon maximum  
79 depositional age analysis. The tendency for the youngest U-Pb dates in a sample to be affected by Pb loss (or other similar



80 process) complicates even conservative estimates of the maximum depositional age (Dickinson and Gehrels., 2009; Coutts et  
81 al., 2019; Schwartz et al., 2022). If apparent Pb loss follows a continuous distribution (e.g., Fig. 3d), then it is ill-advised to  
82 assume that outlying U-Pb dates may be rejected while the rest are considered unperturbed (see also discussion in Copeland,  
83 2020). Even an interpretation based on the peak age probability of the youngest age mode is likely to be too young, because  
84 the process of convolution produces a young shift in the mode of the distribution, in addition to creating a young tail (Fig. 3d;  
85 Fig. A1). Because existing methods of calculating the maximum depositional age (Dickinson and Gehrels, 2009; Coutts et al.,  
86 2019; Vermeesch, 2021) do not account for systematic negative age offsets, our analysis suggests that there is a higher  
87 probability for erroneous estimates of the maximum depositional age if (1) there are a large number of zircon crystals with  
88 crystallization ages that are close to the age of deposition, (2) the overall number of measured U-Pb analyses is very high,  
89 and/or (3) the magnitude of apparent Pb loss is high. In addition, a heavy-tailed distribution of apparent Pb loss (i.e.,  $W_2/W_1$   
90  $\gg 1$ ) will result in a greater probability of finding extremely offset  $Pb^*/U$  values.

91

## 92 **6 Conclusions**

93 This study presents a mathematical framework for quantifying the distribution of apparent Pb loss on U-Pb date distributions,  
94 which could include true loss of radiogenic Pb or other processes that also produce a systematically negative age offset. We  
95 show that a Pb loss-perturbed U-Pb date distribution from a set of zircon crystals with a shared crystallization age can be  
96 represented by the convolution of a Gaussian distribution that reflects measurement uncertainty in  $Pb^*/U$  with a distribution  
97 that characterizes Pb loss,  $g(t)$ . Our approach relies on analyzing differences between the untreated  $Pb^*/U$  distribution from  
98 *in-situ* U-Pb geochronology (i.e., LA-ICP-MS or SIMS) and an independent estimate of the true crystallization age, which  
99 could include U-Pb dates from a thermally annealed and chemically abraded aliquot of the same sample or from another  
00 geochronometer (e.g.,  $^{40}Ar/^{39}Ar$ ). We suggest that the first and second Wasserstein distances ( $W_1$  and  $W_2$ ) of the apparent Pb  
01 loss distribution can be used to quantify the total degree of apparent Pb loss that a set of zircon analyses has undergone, with  
02 maximum possible  $W_1$  and  $W_2$  values of 100.

03

04 We apply this modeling framework to ten igneous samples (Miocene to Carboniferous) analyzed with LA-ICP-MS or SIMS.  
05 All but one of the samples showed a high probability that the untreated U-Pb date distribution has been perturbed by Pb loss  
06 or other equivalent process. Although our analysis shows that multiple parameterizations of  $g(t)$  can achieve statistically  
07 acceptable fits (i.e., K-S or Kuiper  $p$ -value  $>0.05$ ), we suggest that the logit-normal distribution may be a reasonable choice  
08 for exploratory modeling of apparent Pb loss distributions. However, we caution that the number of analyses in the samples  
09 we analyzed was generally low (17-144, average of 39); future efforts to characterize  $g(t)$  may be promoted by collection of  
10 larger- $n$  datasets and through development of nonparametric methods of estimating  $g(t)$ . Furthermore, our estimates of  $g(t)$   
11 should be viewed as minimum estimates of the true amount of Pb lost, as we assumed present-day Pb loss in our analysis.

12 These caveats aside, we noted two behaviors of apparent Pb loss; samples with a bulk shift in U-Pb date distributions ( $W_2/W_1$   
13  $\lesssim 1.3$ ) and samples where most analyses had very little offset but fewer had much larger offsets ( $W_2/W_1 \gtrsim 1.6$ ). The overall  
14 magnitude of  $Pb^*/U$  decrease was also found to be variable, with median values varying from -0.9% to -6.4%.

15

16 Given the widespread application of *in-situ* U-Pb geochronology of untreated zircon across many disciplines of geosciences,  
17 improved characterization of both the distribution type(s) and magnitude of apparent Pb loss is warranted, particularly for  
18 Phanerozoic zircon where cryptic Pb loss is difficult to identify. We highlight a need for increased sampling and high- $n$   
19 characterization of paired non-CA and CA *in-situ* U-Pb datasets. In addition, we recommend simultaneous collection of  
20 parameters such as zircon size and trace elemental concentrations to aid in future efforts to understand the mechanisms of  
21 negative age offsets. Ultimately, we anticipate that improved characterization of the magnitude of apparent Pb loss will aid in  
22 interpreting non-CA *in-situ* U-Pb datasets and guide strategies for future data collection.

### 23 **Data availability**

24 Data are archived under <https://doi.org/10.5281/zenodo.8302521>. Appendix A provides a description of exploratory modeling  
25 of different parameterizations of  $g(t)$ . Figure A1 includes examples of eight continuous distribution types not explored in the  
26 main text. Table A1 and Figure A2 include summaries of all model results. Table A2 presents a summary of model fit for each  
27 sample and distribution type considered. Tables A3 and A4 provide U-Pb analytical results for sample MM20-EC-109 from  
28 the University of Arizona LaserChron Center (LA-ICP-MS) and Boise State University Isotope Geology Laboratory (CA-ID-  
29 TIMS), respectively. Figure A3 includes CL images from the University of Arizona LaserChron Center. Supplemental Video  
30 1 provides an example of convolution. Supplemental Video 2 presents an exploration of the parameter space for the logit-  
31 normal distribution.

32

### 33 **Code availability**

34 Code used in this research is available on GitHub ([https://github.com/grsharman/Pb\\_loss\\_modeling](https://github.com/grsharman/Pb_loss_modeling)) with the v2.0.0 commit  
35 archived under <https://doi.org/10.5281/zenodo.8302313>.

36

### 37 **Video supplement**

38 Supplemental Video 1 is available at <https://doi.org/10.5281/zenodo.8302521>. This animation provides an illustration of how  
39 a Gaussian distribution of U-Pb dates (solid, blue line),  $f(t)$ , may be perturbed by logit-normal Pb loss,  $g(t)$  (solid, red line).  
40 The Pb loss distribution is first reflected about the y-axis and then iteratively shifted by small values of  $t$ ,  $g(t-\tau)$  (dashed, red  
41 line). The convolution of  $f(t)$  and  $g(t)$  at any given value of  $t$  equals the summed area underneath the product of  $f(t)$  and  $g(t-\tau)$ .  
42 Supplemental Video 2 is also available at <https://doi.org/10.5281/zenodo.8302521> and illustrates how the logit-normal  
43 distribution varies with respect to its two parameters  $\mu$  and  $\sigma$ . Note that we have rescaled the x-axis of the logit-normal  
44 distribution such that  $-100 < x < 0$ .

45

### 46 **Author contribution**

47 G. Sharman and M. Malkowski co-designed the study. G. Sharman developed the code. M. Malkowski produced the U-Pb  
48 data from sample MM20-EC-109. G. Sharman and M. Malkowski wrote the manuscript.

49

50 **Competing interests**

51 The authors declare that they have no conflict of interest.

52

53 **Acknowledgments**

54 That authors thank Mark Pecha, George Gehrels, and staff at the University of Arizona LaserChron (supported by NSF-EAR  
55 awards #1649254 and #2050246) as well as Jim Crowley and Mark Schmitz at the Isotope Geology Laboratory at Boise State  
56 University. The project is supported in part by NSF EAR award #2243685, American Chemical Society Petroleum Research  
57 Fund award #66408-DNI8, and the industrial affiliate members of the Detrital Geochronological Laboratory. We thank Kevin  
58 Befus for coding advice. This work benefited from discussions with Alex Lipp and Greg Dumond. Comments and suggestions  
59 from two anonymous reviewers and associate editor Pieter Vermeesch resulted in substantial improvements to the manuscript.

60 **References**

- 61 Aitchison, J., and Bacon-Shone, J.: Convex linear combinations of compositions, *Biometrika*, 86, 351-364,  
62 <https://www.jstor.org/stable/2673517>, 1999.
- 63 Aitchison, J., and Shen, S. M.: Logistic-normal distributions: Some properties and uses, *Biometrika*, 67, 261-272,  
64 <https://www.jstor.org/stable/2335470>, 1980.
- 65 Allen, C. M. and Campbell, I. H.: Identification and elimination of a matrix-induced systematic error in LA-ICP-MS  
66  $^{206}\text{Pb}/^{238}\text{U}$  dating of zircon, *Chemical Geology*, 332, 157-165, 2012.
- 67 Anderson, T.: Correction of common lead in U-Pb analyses that do not report  $^{204}\text{Pb}$ , *Chemical Geology*, 192, 59-79, 2002.
- 68 Andersen, T. and Elburg, M. A.: Open-system behaviour of detrital zircon during weathering: an example from the  
69 Palaeoproterozoic Pretoria Group, South Africa, *Geological Magazine*, 159, 561-576, 2022.
- 70 Andersen, T., Elburg, M. A. and Magwaza, B. N.: Sources of bias in detrital zircon geochronology: Discordance, concealed  
71 lead loss and common lead correction, *Earth-Science Reviews*, 197, 102899, 2019.
- 72 Ashwal, L. D., Tucker, R. D., and Zinner, E. K.: Slow cooling of deep crustal granulites and Pb-loss in zircon, *Geochimica et*  
73 *Cosmochimica Acta*, 63, 2839-2851, 1999.
- 74 Balan, E., Neuville, D. R., Trocellier, P., Fritsch, E., Muller, J. P., and Calas, G.: Metamictization and chemical durability of  
75 detrital zircon, *Am. Mineral.*, 86, 1025-1033, 2001.
- 76 Black, L. P.: Recent Pb loss in zircon: A natural or laboratory induced phenomenon?, *Chem. Geol. Isotope Geoscience section*,  
77 65, 25-33, 1987.
- 78 Blackburn, T., Bowring, S. A., Schoene, B., Mahan, K., and Dudas, F.: U-Pb thermochronology: creating a temporal record  
79 of lithosphere thermal evolution, *Contrib. Mineral. Petrol.*, 162, 479-500, [https://doi.org/10.1007/s00410-011-](https://doi.org/10.1007/s00410-011-0607-6)  
80 [0607-6](https://doi.org/10.1007/s00410-011-0607-6), 2011.
- 81 Bowring, S. A. and Schmitz, M. D.: High-precision U-Pb zircon geochronology and the stratigraphic record, *Rev. Mineral.*  
82 *Geochemistry*, 53, 305-326, 2003.
- 83 Burgess, S. D., Bowring, S., and Shen, S. Z.: High-precision timeline for Earth's most severe extinction, *Proc. Natl. Acad. Sci.*  
84 *U. S. A.*, 111, 3316-3321, 2014.
- 85 Cherniak, D. J. and Watson, E. B.: Pb diffusion in zircon, *Chem. Geol.*, 172, 5-24, 2001.
- 86 Copeland, P.: On the use of geochronology of detrital grains in determining the time of deposition of clastic sedimentary strata,  
87 *Basin Research*, 32, 1532-1546, 2020.
- 88 Compston, W.: Interpretations of SHRIMP and isotope dilution zircon ages for the geological time-scale: I. The early  
89 Ordovician and late Cambrian, *Mineral. Mag.*, 64, 43-57, 2000a.
- 90 Compston, W.: Interpretation of SHRIMP and isotope dilution zircon ages for the Palaeozoic time-scale: II. Silurian to  
91 Devonian, *Mineral. Mag.*, 64, 1127-1171, 2000b.

92 Coutts, D. S., Matthews, W. A., and Hubbard, S. M.: Assessment of widely used methods to derive depositional ages from  
93 detrital zircon populations, *Geosci. Front.*, 34, 1421-1435, 2019.

94 Crowley, Q. G., Heron, K., Riggs, N., Kamber, B., Chew, D., McConnell, B., and Benn, K.: Chemical abrasion applied to LA-  
95 ICP-MS U–Pb zircon geochronology, 4, 503–518, 2014.

96 Davis, D.W., Williams, I.S., and Krogh, T.E.: Historical development of zircon geochronology, *Reviews in Mineralogy and*  
97 *Geochemistry*, 53, 145-181, <https://doi.org/10.2113/0530145>, 2003.

98 Dickinson, W. R. and Gehrels, G. E.: Use of U–Pb ages of detrital zircons to infer maximum depositional ages of strata: A test  
99 against a Colorado Plateau Mesozoic database, *Earth Planet. Sci. Lett.*, 288, 115–125, 2009.

00 Froude, D. O., Ireland, T. R., Kinny, P. D., Williams, I. S., Compston, W., Williams, I. R., and Myers, J. S.: Ion microprobe  
01 identification of 4,100–4,200 Myr-old terrestrial zircons, *Nature*, 304, 616, 1983.

02 Geisler, T., Pidgeon, R. T., Van Bronswijk, W., and Kurtz, R.: Transport of uranium, thorium, and lead in metamict zircon  
03 under low-temperature hydrothermal conditions, *Chem. Geol.*, 191, 141–154, 2002.

04 Geisler, T., Pidgeon, R. T., Kurtz, R., van Bronswijk, W., and Schleicher, H.: Experimental hydrothermal alteration of partially  
05 metamict zircon, *Am. Mineral.*, 88, 1496–1513, 2003.

06 Gehrels, G. E.: Detrital Zircon U-Pb Geochronology Applied to Tectonics, *Annu. Rev. Earth Planet. Sci.*, 42, 127–149, 2014.

07 Gehrels, G., Giesler, D., Olsen, P., Kent, D., Marsh, A., Parker, W., Rasmussen, C., Mundil, R., Irmis, R., Geissman, J., and  
08 Lepre, C.: LA-ICPMS U–Pb geochronology of detrital zircon grains from the Coconino, Moenkopi, and Chinle  
09 formations in the Petrified Forest National Park (Arizona), 2, 257–282, 2020.

10 Gradstein, F. M., Ogg, J. G., Smith, A. G., Bleeker, W., and Lourens, L. J.: A new Geologic Time Scale, with special reference  
11 to Precambrian and Neogene, *Episodes*, 27, 83–100, 2004.

12 Grushka, E.: Characterization of Exponentially Modified Gaussian Peaks in Chromatography, *Anal. Chem.*, 44, 1733–1738,  
13 1972.

14 Herriott, T. M., Crowley, J. L., Schmitz, M. D., Wartes, M. A., and Gillis, R. J.: Exploring the law of detrital zircon: LA-ICP-  
15 MS and CA-TIMS geochronology of Jurassic forearc strata, Cook Inlet, Alaska, USA, 47, 1044-1048, 2019.

16 Howard, B., Sharman, G., Crowley, J. L., and Wersan, E. R.: The instrumentation dilemma: A comparison of paired LA-ICP-  
17 MS and ID-TIMS U-Pb dates from zircon, *Geological Society of America Abstracts with Programs*, 54, 2022.

18 Ireland, T. R. and Williams, I. S.: Considerations in zircon geochronology by SIMS, *Rev. Mineral. Geochemistry*, 53, 215–  
19 241, 2003.

20 Johnstone, S. A., Schwartz, T. M., and Holm-Denoma, C. S.: A Stratigraphic Approach to Inferring Depositional Ages From  
21 Detrital Geochronology Data, 7, article 57, 2019.

22 Kaufmann, B.: Calibrating the Devonian Time Scale: A synthesis of U-Pb ID-TIMS ages and conodont stratigraphy, *Earth-  
23 Science Rev.*, 76, 175–190, 2006.

24 Kirkland, C. L., Abello, F., Danišik, M., Gardiner, N.J., and Spencer, C.: Mapping temporal and spatial patterns of zircon U-  
25 Pb disturbance: A Yilgarn Craton case study, *Gondwana Research*, 52, 39-47,  
26 <https://dx.doi.org/10.1016/j.gr.2017.08.004>, 2017.

27 Kirland, C. L., Barnham, M., and Danišik, M.: Find a match with triple-dating: Antarctic sub-ice zircon detritus on the modern  
28 shore of Western Australia, *Earth and Planetary Science Letters*, 531, 115953,  
29 <https://doi.org/10.1016/j.epsl.2019.115953>, 2020.

30 Kröner, A., Jaekel, P., and Williams, I. S.: Pb-loss patterns in zircons from a high-grade metamorphic terrain as revealed by  
31 different dating methods: U-Pb and Pb-Pb ages for igneous and metamorphic zircons from northern Sri Lanka,  
32 *Precambrian Res.*, 66, 151–181, 1994.

33 Kryza, R., Crowley, Q. G., Larionov, A., Pin, C., Oberc-Dziedzic, T., and Mochnacka, K.: Chemical abrasion applied to  
34 SHRIMP zircon geochronology: An example from the Variscan Karkonosze Granite (Sudetes, SW Poland),  
35 *Gondwana Res.*, 21, 757–767, 2012.

36 Lipp, A.G., and Vermeesch, P.: Short communication: The Wasserstein distance as a dissimilarity metric for comparing detrital  
37 age spectra and other geological distributions, *Geochronology*, 5, 263-270, [https://doi.org/10.5194/gchron-5-263-](https://doi.org/10.5194/gchron-5-263-2023)  
38 2023, 2023.

39 Marsellos, A. E. and Garver, J. I.: Radiation damage and uranium concentration in zircon as assessed by Raman spectroscopy  
40 and neutron irradiation, *Am. Mineral.*, 95, 1192–1201, 2010.

- 41 Mattinson, J. M.: Zircon U-Pb chemical abrasion (“CA-TIMS”) method: Combined annealing and multi-step partial  
42 dissolution analysis for improved precision and accuracy of zircon ages, *Chem. Geol.*, 220, 47–66, 2005.
- 43 Mead, R.: A generalized logit-normal distribution, *Biometrics*, 21, 721-732, <https://www.jstor.org/stable/2528553>,  
44 1965.
- 45 Mezger, K. and Krogstad, J. E.: Interpretation of discordant U-Pb zircon ages: An evaluation, *J. Metamorph. Geol.*, 15, 127–  
46 140, 1997.
- 47 Miller, J. S., Matzel, J. E. P., Miller, C. F., Burgess, S. D., and Miller, R. B.: Zircon growth and recycling during the assembly  
48 of large, composite arc plutons, *J. Volcanol. Geotherm. Res.*, 167, 282–299, 2007.
- 49 Miller, E. L., Raftrey, M. E., and Lund Snee, J.-E.: Downhill from Austin and Ely to Las Vegas: U-Pb detrital zircon suites  
50 from the Eocene–Oligocene Titus Canyon Formation and associated strata, Death Valley, California, *Geol. Soc. Am.*  
51 *Spec. Pap.*, 555, 359-378, 2022.
- 52 Morris, G. A., Kirkland, C. L., and Pease, V.: Orogenic paleofluid flow recorded by discordant detrital zircons in the  
53 Caledonian foreland basin of northern Greenland, 7, 138–143, 2015.
- 54 Nasdala, L., Hanchar, J. M., Kronz, A., and Whitehouse, M. J.: Long-term stability of alpha particle damage in natural zircon,  
55 *Chem. Geol.*, 220, 83–103, 2005.
- 56 Orejana, D., Merino Martínez, E., Villaseca, C., and Andersen, T.: Ediacaran-Cambrian paleogeography and geodynamic  
57 setting of the Central Iberian Zone: Constraints from coupled U-Pb-Hf isotopes of detrital zircons, *Precambrian Res.*,  
58 261, 234–251, 2015.
- 59 Pidgeon, R. T., O’Neil, J. R., and Silver, L. T.: Uranium and lead isotopic stability in metamict zircon under experimental  
60 hydrothermal conditions, *Science*, 154, 1538-1540, <https://www.jstor.org/stable/1720453>, 1966.
- 61 Pidgeon, R. T., Nemchin, A. A., and Whitehouse, M. J.: The effect of weathering on U-Th-Pb and oxygen isotope systems of  
62 ancient zircons from the Jack Hills, Western Australia, *Geochim. Cosmochim. Acta*, 197, 142–166, 2017.
- 63 Pidgeon, R. T., Nemchin, A. A., Roberts, M. P., Whitehouse, M. J., and Bellucci, J. J.: The accumulation of non-formula  
64 elements in zircons during weathering: Ancient zircons from the Jack Hills, Western Australia, *Chem. Geol.*, 530,  
65 119310, <https://doi.org/10.1016/j.chemgeo.2019.119310>, 2019.
- 66 Press, W. H., Teukolsky, S. A., Vetterling, W. T., and Flannery, B. P.: *Numerical Recipes: The Art of Scientific Computing*,  
67 3rd Editio., Cambridge University Press, 1235 pp., 2007.
- 68 Puetz, S. J., Spencer, C. J., and Ganade, C. E.: Analyses from a validated global U–Pb detrital zircon database: Enhanced  
69 methods for filtering discordant U–Pb zircon analyses and optimizing crystallization age estimates, *Earth-Science*  
70 *Rev.*, 220, 103745, <https://doi.org/10.1016/j.earscirev.2021.103745>, 2021.
- 71 Pullen, A., Ibáñez-Mejía, M., Gehrels, G. E., Ibáñez-Mejía, J. C., and Pecha, M.: What happens when  $n=1000$ ? Creating large-  
72  $n$  geochronological datasets with LA-ICP-MS for geologic investigations, *J. Anal. At. Spectrom.*, 29, 971–980, 2014.
- 73 Reimink, J. R., Davies, J. H. F. L., Waldron, J. W. F., and Rojas, X.: Dealing with discordance: A novel approach for analysing  
74 U–Pb detrital zircon datasets, *J. Geol. Soc. London.*, 173, 577–585, 2016.
- 75 Rioux, M., Bowring, S., Kelemen, P., Gordon, S., Dudás, F., and Miller, R.: Rapid crustal accretion and magma assimilation  
76 in the Oman-U.A.E. ophiolite: High precision U-Pb zircon geochronology of the gabbroic crust, *J. Geophys. Res.*  
77 *Solid Earth*, 117, 2012.
- 78 Rossignol, C., Hallot, E., Bourquin, S., Poujol, M., Jolivet, M., Pellenard, P., Ducassou, C., Nalpas, T., Heilbronn, G., Yu, J.,  
79 and Dabard, M. P.: Using volcanoclastic rocks to constrain sedimentation ages: To what extent are volcanism and  
80 sedimentation synchronous?, *Sediment. Geol.*, 381, 46–64, 2019.
- 81 Ruiz, M., Schaltegger, U., Gaynor, S. P., Chiaradia, M., Abrecht, J., Gislser, C., Giovanoli, F., and Wiederkehr, M.: Reassessing  
82 the intrusive tempo and magma genesis of the late Variscan Aar batholith: U–Pb geochronology, trace element and  
83 initial Hf isotope composition of zircon, *Swiss J. Geosci.*, 115, 1–24, 2022.
- 84 Saylor, J. E. and Sundell, K. E.: Quantifying comparison of large detrital geochronology data sets, 12, 203–220,  
85 <https://doi.org/10.1130/GES01237.1>, 2016.
- 86 Schoene, B., Guex, J., Bartolini, A., Schaltegger, U., and Blackburn, T. J.: Correlating the end-Triassic mass extinction and  
87 flood basalt volcanism at the 100 ka level, *Geology*, 38, 387–390, <https://doi.org/10.1130/G30683.1>, 2010. Schoene,  
88 B., Schaltegger, U., Brack, P., Latkoczy, C., Stracke, A., and Günther, D.: Rates of magma differentiation and  
89 emplacement in a ballooning pluton recorded by U-Pb TIMS-TEA, Adamello batholith, Italy, *Earth Planet. Sci. Lett.*,  
90 355–356, 162–173, 2012.

91 Schoene, B.: U-Th-Pb Geochronology, *Treatise on Geochemistry* (Second Edition), 4, 341–378, 2013.

92 Schwartz, T. M., Souders, A. K., Lundstern, J.-E., Gilmer, A. K., and Thompson, R. A.: Revised age and regional correlations  
93 of Cenozoic strata on Bat Mountain, Death Valley region, California, USA, from zircon U-Pb geochronology of  
94 sandstones and ash-fall tuffs, *Geosphere*, 19, 235–257, 2022.

95 Sharman, G. R., Covault, J. A., Flaig, P. P., Dunn, R., Fussee-Durham, P., Larson, T. E., Shanahan, T. M., Dubois, K., Shaw,  
96 J. B., Crowley, J. L., Shaulis, B.: Coastal response to global warming during the Paleocene-Eocene Thermal Maximum,  
97 625, 111664, <https://doi.org/10.1016/j.palaeo.2023.111664>, 2023.

98 Silver, L. T. and Deutsch, S.: Uranium-Lead Isotopic Variations in Zircons: A Case Study, *J. Geol.*, 71, 721–758, 1963.

99 Snow, J. K. and Lux, D. R.: Tectono-sequence stratigraphy of Tertiary rocks in the Cottonwood Mountains and northern Death  
00 Valley area, California and Nevada, *Geol. Soc. Am. Spec. Pap.*, 333, 17–64, 1999.

01 Solari, L. A., Ortega-Obregón, C., and Bernal, J. P.: U-Pb zircon geochronology by LAICPMS combined with thermal  
02 annealing: Achievements in precision and accuracy on dating standard and unknown samples, *Chem. Geol.*, 414,  
03 2015.

04 Spencer, C. J., Kirkland, C. L., and Taylor, R. J. M.: Strategies towards statistically robust interpretations of in situ U-Pb zircon  
05 geochronology, *Geosci. Front.*, 7, 581–589, 2016.

06 Stern, T. W., Goldich, S. S., and Newell, M. F.: Effects of weathering on the U-Pb ages of zircon from the Morton Gneiss,  
07 Minnesota, *Earth Planet. Sci. Lett.*, 1, 369–371, 1966.

08 Sundell, K. E., Gehrels, G. E., and Pecha, M. E.: Rapid U-Pb Geochronology by Laser Ablation Multi-Collector ICP-MS,  
09 *Geostand. Geoanalytical Res.*, 45, 37–57, 2021.

10 Tilton, G. R., Patterson, C., Brown, H., Ingham, M., Hayden, R., Hess, D., and Larsen, E., J.: Isotopic composition and  
11 distribution of lead, uranium, and thorium in a Precambrian granite, *Bull. Geol. Soc. Am.*, 66, 1131–1148, 1955.

12 Ver Hoeve, T. J., Scoates, J. S., Wall, C. J., Weis, D., and Amini, M.: Evaluating downhole fractionation corrections in LA-  
13 ICP-MS U-Pb zircon geochronology, *Chem. Geol.*, 483, 201–217, 2018.

14 Vermeesch, P.: Dissimilarity measures in detrital geochronology, *Earth-Science Rev.*, 178, 310–321, 2018a.

15 Vermeesch, P.: Statistical models for point-counting data, *Earth-Science Rev.*, 501, 112–118, 2018b.

16 Vermeesch, P.: Maximum depositional age estimation revisited, *Geosci. Front.*, 12, 843–850, 2021.

17 von Quadt, A., Gallhofer, D., Guillong, M., Peytcheva, I., Waelle, M., and Sakata, S.: U-Pb dating of CA/non-CA treated  
18 zircons obtained by LA-ICP-MS and CA-TIMS techniques: Impact for their geological interpretation, *J. Anal. At.*  
19 *Spectrom.*, 29, 1618–1629, 2014.

20 Watts, K. E., Coble, M. A., Vazquez, J. A., Henry, C. D., Colgan, J. P. and John, D. A.: Chemical abrasion-SIMS (CA-SIMS)  
21 U-Pb dating of zircon from the late Eocene Caetano caldera, Nevada *Chemical Geology*, 439, 139–151, 2016.

22 Wetherill, G. W.: Discordant Uranium-Lead Ages, 1, *Trans. Am. Geophys. Union*, 37, 320–326, 1956.

23 Willner, A. P., Sindern, S., Metzger, R., Ermolaeva, T., Kramm, U., Puchkov, V., and Kronz, A.: Typology and single grain  
24 U/Pb ages of detrital zircons from Proterozoic sandstones in the SW Urals (Russia): Early time marks at the eastern  
25 margin of Baltica, *Precambrian Res.*, 124, 1–20, 2003.

26 Zeh, A., Wilson, A. H., and Ovtcharova, M.: Source and age of upper Transvaal Supergroup, South Africa: Age-Hf isotope  
27 record of zircons in Magaliesberg quartzite and Dullstroom lava, and implications for Paleoproterozoic (2.5–2.0 Ga)  
28 continent reconstruction, *Precambrian Res.*, 278, 1–21, 2016.